

# Computational dosimetry of induced electric fields during realistic movements in the vicinity of a 3 T MRI scanner

Ilkka Laakso<sup>1</sup>, Sami Kännälä<sup>2</sup> and Kari Jokela<sup>2</sup>

<sup>1</sup> Department of Computer Science and Engineering, Nagoya Institute of Technology, Nagoya, Japan

<sup>2</sup> STUK—Radiation and Nuclear Safety Authority, Helsinki, Finland

E-mail: [laakso.ilkka@nitech.ac.jp](mailto:laakso.ilkka@nitech.ac.jp) and [sami.kannala@stuk.fi](mailto:sami.kannala@stuk.fi)

Received 31 January 2013, in final form 2 March 2013

Published 2 April 2013

Online at [stacks.iop.org/PMB/58/2625](http://stacks.iop.org/PMB/58/2625)

## Abstract

Medical staff working near magnetic resonance imaging (MRI) scanners are exposed both to the static magnetic field itself and also to electric currents that are induced in the body when the body moves in the magnetic field. However, there are currently limited data available on the induced electric field for realistic movements. This study computationally investigates the movement induced electric fields for realistic movements in the magnetic field of a 3 T MRI scanner. The path of movement near the MRI scanner is based on magnetic field measurements using a coil sensor attached to a human volunteer. Utilizing realistic models for both the motion of the head and the magnetic field of the MRI scanner, the induced fields are computationally determined using the finite-element method for five high-resolution numerical anatomical models. The results show that the time-derivative of the magnetic flux density ( $dB/dt$ ) is approximately linearly proportional to the induced electric field in the head, independent of the position of the head with respect to the magnet. This supports the use of  $dB/dt$  measurements for occupational exposure assessment. For the path of movement considered herein, the spatial maximum of the induced electric field is close to the basic restriction for the peripheral nervous system and exceeds the basic restriction for the central nervous system in the international guidelines. The 99th percentile electric field is a considerably less restrictive metric for the exposure than the spatial maximum electric field; the former is typically 60–70% lower than the latter. However, the 99th percentile electric field may exceed the basic restriction for  $dB/dt$  values that can be encountered during tasks commonly performed by MRI workers. It is also shown that the movement-induced eddy currents may reach magnitudes that could electrically stimulate the vestibular system, which could play a significant

role in the generation of vertigo-like sensations reported by people moving in a strong static magnetic field.

 Online supplementary data available from [stacks.iop.org/PMB/58/2625/mmedia](https://stacks.iop.org/PMB/58/2625/mmedia)

(Some figures may appear in colour only in the online journal)

## 1. Introduction

Humans moving in strong static magnetic fields of magnetic resonance imaging (MRI) systems may experience mild sensory effects, including vertigo, nausea, headache, metallic taste in mouth, and rarely magnetophosphenes (Schenck 2000, de Vocht *et al* 2006, Weintraub *et al* 2007, Heilmaier *et al* 2011). For patients undergoing MRI examination, the most frequently observed sensation among these is vertigo (Weintraub *et al* 2007, Heilmaier *et al* 2011). Because these effects are mild and transient, static magnetic field of MRI is not considered hazardous for patients (Schenck 2000, Shellock and Crues 2004), except for the risk of mechanical injury due to magnetic forces acting on ferromagnetic materials that might be included in certain biomedical implants or devices (Schenck 2000, Shellock and Crues 2004). However, for medical staff or technicians who repeatedly may need to work in the fringe magnetic field and even inside if an MRI scanner, vertigo or other potential sensory effects may be annoying and might possibly impair working ability (van Nierop *et al* 2012, Jokela and Saunders 2011). Currently, international guidelines for limiting the exposure of workers moving in static magnetic fields are in preparation (ICNIRP 2012).

The effects of static magnetic fields are caused by two related factors. The first factor is the exposure to a static magnetic field itself. As shown by Roberts *et al* (2011), a strong static magnetic field can directly affect the vestibular function, which could explain sensations of vertigo. Roberts *et al* (2011) attributed this effect to the Lorentz force that acts on ionic currents that constantly flow in the endolymphic fluid of the labyrinth of the inner ear. The second factor is the exposure to the electric fields/currents that are induced in the human body moving in a static magnetic field. If the induced currents are strong enough, they may stimulate excitable nerve, muscle, or receptor cells. Preventing the stimulation of the central nervous system (CNS) or peripheral nerves has been the biological basis for deriving the basic restrictions in the ICNIRP (2010) guidelines for the exposure to low-frequency electromagnetic fields. Weak direct currents can also affect the vestibular function as is evident from the studies of galvanic vestibular stimulation (GVS) (Fitzpatrick and Day 2004). Consequently, if the magnitude of movement-induced currents were comparable to the currents used in GVS, they could electrically stimulate the vestibular system resulting in sensations of vertigo. As discussed by Glover *et al* (2007), the magnetic-field related vertigo might actually be attributable to the combination of both static magnetic field acting on the vestibular system and GVS-like stimulation by movement-induced currents.

The exposure of workers to the static and gradient fields of MRI scanners have been successfully investigated using measurements (Bradley *et al* 2007, Fuentes *et al* 2008, de Vocht *et al* 2009, Glover and Bowtell 2008, Kännälä *et al* 2009). However, for assessing the exposure to movement-induced electric fields, computational techniques are needed. These techniques have been utilized in several studies (Liu *et al* 2003, Crozier and Liu 2005, Ilvonen and Laakso 2009, Cobos Sánchez *et al* 2009, Chiampi and Zilberti 2011, Cobos Sánchez *et al* 2012). From these studies, it is clear that the magnitude of movement induced electric fields can be within



**Figure 1.** Volunteer leaning into the magnet bore during magnetic field measurements.

the same order of magnitude as the basic restrictions set by international guidelines or standards (ICNIRP 2010, IEEE 2002). Various different models for the human anatomy have been used: a homogeneous model of the whole body was employed in Chiampi and Zilberti (2011), a 4 or 6 mm resolution whole-body model in Liu *et al* (2003) and Crozier and Liu (2005), a three-domain model of the head in Cobos Sánchez *et al* (2009) and Cobos Sánchez *et al* (2012), and four different heterogeneous anatomical models of the head with 2 mm or 1 mm resolution in Ilvonen and Laakso (2009). Some of the studies have used realistic models for the magnetic field of the MRI magnet (Liu *et al* 2003, Crozier and Liu 2005, Chiampi and Zilberti 2011), while others have employed simple analytical expressions for the magnetic field. However, all previous studies have only considered idealized translational or rotational movements. Additionally, Cobos Sánchez *et al* (2012) have shown that Liu *et al* (2003) and Crozier and Liu (2005) have used a formulation that gives correct results only for the special case of purely translational motion.

In this study, movement induced fields are computationally investigated for realistic motion in the vicinity of an MRI scanner. The path of movement is based on magnetic field measurements using a coil sensor attached to a human volunteer whose movements simulated those of a medical worker (Kännälä *et al* 2009). Utilizing realistic models for both the motion of the head and the magnetic field of the MRI scanner, the induced fields are determined computationally for five high-resolution numerical anatomical models. The computed induced electric fields are then compared with the exposure limits of ICNIRP (ICNIRP 2009, 2010), and the significance of the results on occupational exposure assessment is discussed. Additionally, the magnitudes of the induced currents are compared with currents that have been used for GVS for roughly estimating the role of induced currents in the generation of magnetic field induced vertigo.

## 2. Models and methods

### 2.1. Magnetic field measurements

The magnetic field measurements were performed in the vicinity of a compact 3.0 T scanner (Philips Achieva 3.0T). The measurement method and results are described in detail in Kännälä *et al* (2009). A sensor consisting of three orthogonal coils was attached to the forehead of a volunteer. During movements near the MRI scanner, the currents induced in the coils were recorded using an oscilloscope, after which the time-derivative of the magnetic flux ( $dB/dt$ ) was determined from the induced currents. The movements of the volunteer simulated the movements of a medical worker positioning a test phantom on the patient bed inside the MRI scanner. An example of the movements of the volunteer during measurements is shown in figure 1.

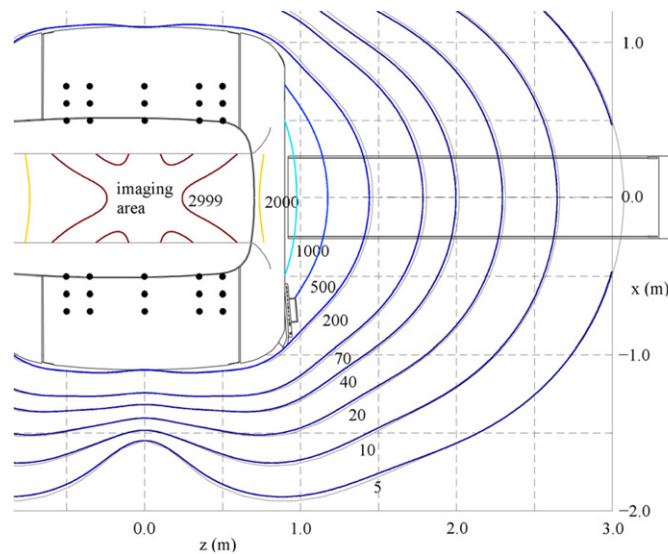


**Figure 2.** Isolines of the magnetic flux density (mT) from the manufacturer data (thin lines) and those obtained using the numerical model of the magnet (thick lines). The dots show the locations of the thin current loops that comprise the numerical model of the magnet.

**Table 1.** Simplified model of the 3.0 T magnet. Currents (kA) of the thin wire loops.

Radius (cm)	Distance from the centre (cm)				
	-50	-35	0	+35	+50
50	-220.5	-1994.0	-2136.9	-1994.0	-220.5
60	2039.1	5571.2	9157.0	5571.2	2039.1
70	-520.8	-3687.6	-5392.4	-3687.6	-520.8

## 2.2. Numerical model of the MRI scanner

The superconducting magnet that produces the magnetic field of the MRI scanner was modelled by means of 15 thin current loops. Each loop was a regular decagon the area of which was equal to a circle with radius shown in table 1. The magnetic field from the loops, each of which consisted of ten straight line segments, was calculated analytically by the Biot–Savart law. The radii and positions of the loops were chosen by trial and error, after which the magnitudes of the loop currents, listed in table 1, were determined by least-squares fitting of the calculated magnetic field to the magnetic field data from the manufacturer. Figure 2 shows a comparison between the distributions of the modelled magnetic field and the magnetic field provided by the manufacturer.

## 2.3. Trajectory of the head

The position and velocity of the magnetic field probe were not tracked during measurements, so the same trajectory as in the measurements could not be reconstructed exactly (there are multiple different trajectories that give the same  $dB/dt$ ). Therefore, a trajectory that gives approximately the same  $dB/dt$  as that in the measurements, and roughly resembles the path of the volunteer was selected. As it was not possible to take into account changes in posture

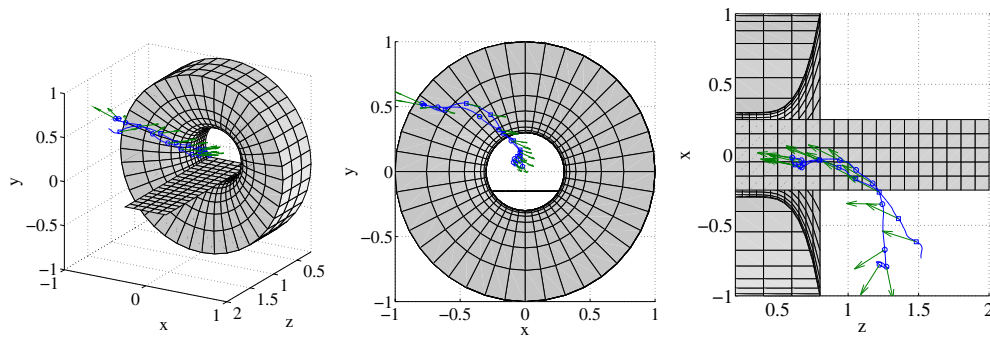


**Figure 3.** Trajectory of the head viewed from the front right (left), front (middle), and above (right). Squares show the path of the centre of rotation of the head when the head is moving into the magnet bore, and circles show the path when the head is moving back from the magnet bore. Arrows show the direction of the head. The time difference between the markers is 0.5 s, and the first and last markers correspond to 1.0 and 10.5 s, respectively.

during the movement, only the head was considered. The head was assumed to be rigid, i.e. deformation of tissues during movement was ignored. Therefore, for simplicity, a single point was defined as the centre of rotation. The point was the intersection of the mid-sagittal plane and a line that passes through the left and right auricular points. This point was chosen because it could be easily and unambiguously determined for multiple different anatomical models. The path of the movement was determined for the head of the DUKE model (section 2.4), but all five head models were assumed to follow the same path of movement, not taking into account differences in height (the height of the volunteer was about 175 cm).

For each point on the trajectory, the location, direction, and translational velocity of the head with respect to the magnet, as well as the angular velocity of the head were determined. The time step was 0.025 s and the number of time steps was 400. The maximum translational and angular accelerations of the head were limited from above by  $a < 5 \text{ m s}^{-2}$  and  $\alpha < 2\pi \text{ rad s}^{-2}$ , respectively. It was also made sure that the location and direction of the head were physically possible. Then the maximum velocity and angular velocity were  $v < 0.75 \text{ m s}^{-1}$  and  $\omega < 2.5 \text{ rad s}^{-1}$ . Figure 3 shows the trajectory of the centre of rotation of the head. First, the head is moving towards the magnet bore, then it slows down and stays approximately stationary near the mouth of the MRI scanner, after this it moves backwards away from the magnet, and finally turns around. A comparison between the measured and modelled magnetic flux densities (calculated in front of the forehead where the magnetic field probe is located) on the chosen trajectory is shown in figure 4.

#### 2.4. Numerical anatomical models

A total of five anatomical voxel models of the head were used. The models were identical to those used in Laakso and Hirata (2012a). They were the Japanese adult male (TARO) and female (HANAKO) models (Nagaoka *et al* 2004), the Virtual Family adult male (DUKE) and female (ELLA) models (Christ *et al* 2010), and the HPA adult male model NORMAN (Dimbylow 1998). The models are illustrated in figure 5. For the TARO, HANAKO, and NORMAN models that consist of  $2 \text{ mm} \times 2 \text{ mm} \times 2 \text{ mm}$  voxels, each of the original voxels was divided evenly into 64 new voxels with a 0.5 mm side length. For the DUKE and ELLA models, a uniform  $0.5 \text{ mm} \times 0.5 \text{ mm} \times 0.5 \text{ mm}$  voxel grid was used. Similarly to Laakso and Hirata (2012a), the eyes of the models were replaced with new more detailed eyes, and the models were

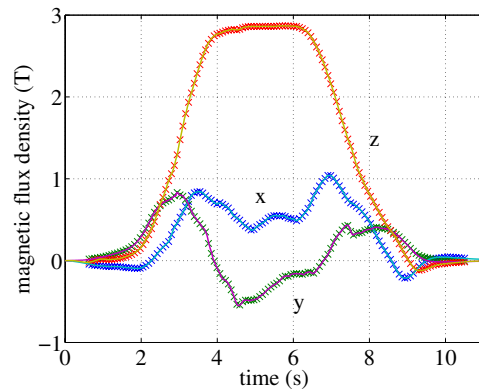


**Figure 4.** Measured and modelled magnetic flux densities. Solid lines show the magnetic flux density determined from measured  $dB/dt$ , and markers show the computed magnetic flux density. For clarity, the figure only shows the markers for every third time step. Components of the magnetic field:  $x$  = lateral,  $y$  = infero-superior,  $z$  = antero-posterior.

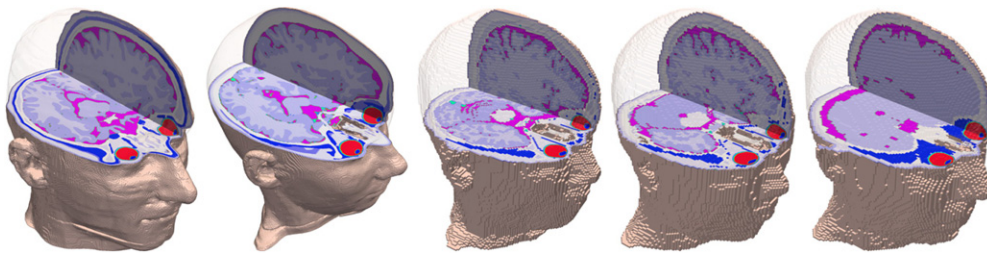


**Figure 5.** False colour images of the DUKE, ELLA, TARO, HANAKO, and NORMAN models (left to right).

‘smoothed’ in order to reduce the effect of numerical error caused by staircase approximation of curved boundaries (Laakso and Hirata 2012c). The total numbers of unique tissues/body fluids (including internal air) in the heads of the DUKE, ELLA, TARO, HANAKO, and NORMAN models were 48, 46, 28, 28, and 16, respectively. Each tissue was assigned a conductivity value, which were similar to those used in our previous study (Laakso and Hirata 2012a). The only difference with the previous study was that the brain of the NORMAN model was given the conductivity of grey matter ( $0.10 \text{ S m}^{-1}$ ). Previously, it had the average conductivity of grey and white matters ( $0.08 \text{ S m}^{-1}$ ). Most of the conductivities, with the exception of ocular tissues and fluids (Lindenblatt and Silny 2001) and the cerebrospinal fluid (Baumann *et al* 1997), were originally obtained from Gabriel (1996).

### 2.5. Determining the induced electric field

In the following, internal movement, such as blood flow, and ionic currents constantly present in the body have been ignored. In a conducting body that is slowly moving in a static magnetic field  $\mathbf{B}_0$ , the current density is

$$\mathbf{J} = \sigma(\mathbf{E} + \mathbf{v} \times \mathbf{B}_0), \quad (1)$$

where  $\sigma$  is the conductivity, and it has been assumed that induced currents do not perturb the external magnetic field. Because the displacement current can be ignored, the current density satisfies the stationary condition (Cobos Sánchez *et al* 2012)

$$\nabla \cdot \mathbf{J} = 0. \quad (2)$$

The external magnetic field is static, so the electric field is irrotational. Consequently, it can be represented as the gradient of the electric scalar potential  $\phi$ , which by (1) and (2) satisfies

$$\nabla \cdot \sigma \nabla \phi = \nabla \cdot (\sigma \mathbf{v} \times \mathbf{B}_0). \quad (3)$$

The right-hand side driving term  $\mathbf{v} \times \mathbf{B}_0$  is calculated in the following way. First, the magnetic flux density  $\mathbf{B}_0$  at each point in the head is calculated analytically using the location and direction of the head with respect to the magnet. Then, the velocity field  $\mathbf{v}$  is determined from the translational and angular velocities of the whole head, and finally, the cross product is calculated. In this work, the scalar potential  $\phi$  is numerically solved from (3) using the finite-element method with first-order corner-based basis functions in cubical elements. The solver is described in detail in Laakso and Hirata (2012b). After the scalar potential has been determined, the induced electric field that is visible to an observer who is co-moving with the head can be calculated by

$$\mathbf{E}' = -\nabla \phi + \mathbf{v} \times \mathbf{B}_0. \quad (4)$$

Note that, as also shown by Bringuier (2003), the approach presented above is equivalent to starting from the stationary Faraday law in the coordinate frame of the head  $\nabla \times \mathbf{E}' = -\frac{\partial}{\partial t} \mathbf{B}'_0$ , and utilizing the time derivative of the magnetic vector potential  $-\frac{\partial}{\partial t} \mathbf{A}'_0$  as the driving term. This is due to the fact that one can choose  $\frac{\partial}{\partial t} \mathbf{A}'_0 = -\mathbf{v} \times \mathbf{B}$ , which can be verified by simple calculation. Therefore, the magnetic field probe, which essentially measures  $\frac{\partial}{\partial t} \mathbf{B}'_0$ , gives correct results both when it is stationary in an alternating magnetic field or when it is moved in a static magnetic field.

## 2.6. Analysis of the induced fields

The electric field in the CNS and other tissues is analysed as recommended by ICNIRP (2010) with modifications described below. First, a vector average of the induced field is taken over  $2 \text{ mm} \times 2 \text{ mm} \times 2 \text{ mm}$  cubical volumes (64 voxels). Then the 99th percentile of this averaged field is calculated. The ICNIRP (2010) guidelines specify that the 99th percentile should be calculated separately for each specific tissue. However, the 99th percentile values calculated in this way depend on the number of tissues in each anatomical model (Bakker *et al* 2012). Because the segmentation of tissues is different in each of the five studied anatomical models, the results would not be consistent between the models. Therefore, instead of calculating the 99th percentile for each tissue separately, the 99th percentile of the average field is calculated over the whole CNS (including retinas and optic nerves) or whole head. In addition to the 99th percentile value over the whole CNS/head, the spatial maximum of the averaged field is calculated over the whole CNS/head. Note that the 99th percentile calculated separately for each tissue falls between the spatial maximum value and the 99th percentile calculated over the whole CNS/head. When calculating the maximum and 99th percentile values, the lowermost 5 cm of the computational domain is ignored in order to remove any errors caused by truncation of the body at the neck.

Total induced eddy current is approximated by integrating the positive (or negative) normal component of the current density over all horizontal, sagittal, and coronal cross section planes, and taking the maximum.

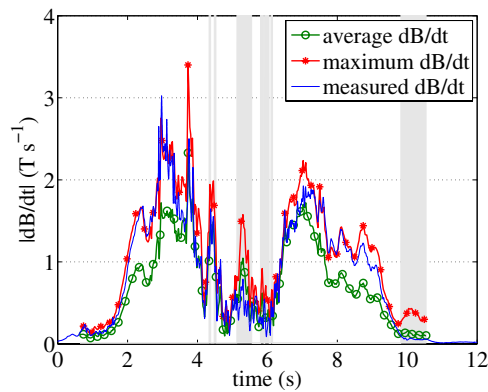


**Figure 6.** The absolute value of the time derivative of the magnetic flux density ( $dB/dt$ ) measured at the magnetic field sensor, the absolute value of the vector average of  $dB/dt$  computed over the whole head, and the maximum computed  $dB/dt$  in the head. Shaded areas show when the average  $dB/dt$  in the head is at least 20% higher than the measured  $dB/dt$  (probe attached to the forehead).

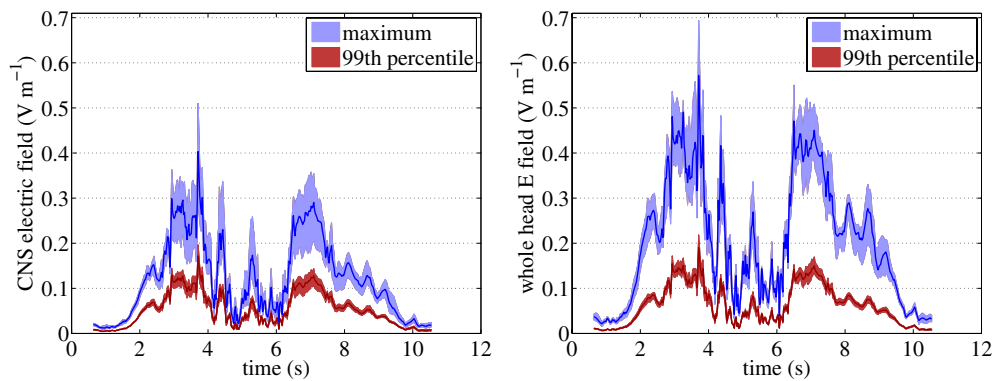
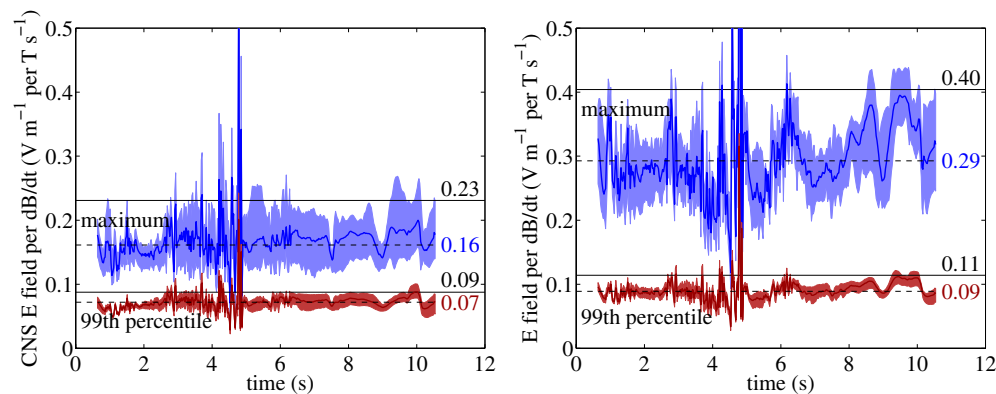


**Figure 7.** The maximum and 99th percentile electric fields in the CNS (left) and in the whole head (right). Solid lines show the average values and the shaded areas depict the ranges of variation over the five anatomical models.

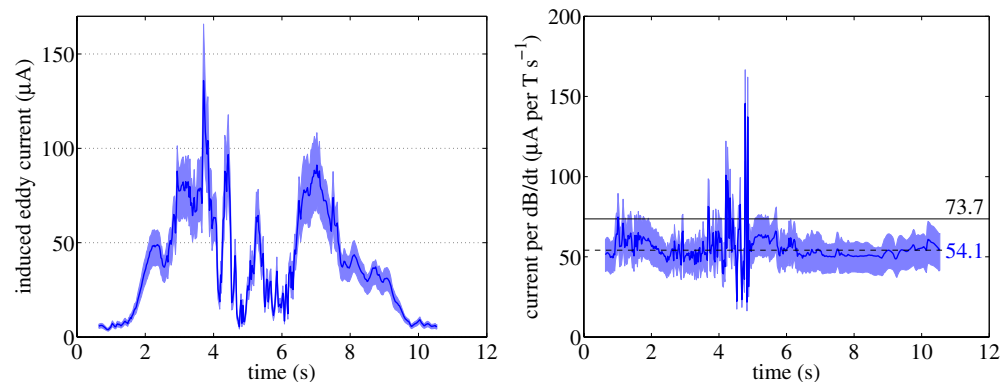
### 3. Results

Figure 6 shows the measured  $dB/dt$  at the measurement probe (forehead) and the maximum and average values of the computed  $dB/dt$  in the head. It seems that the maximum  $dB/dt$  in the head is typically slightly higher than the measured  $dB/dt$ . On the other hand, the average  $dB/dt$  in the head is typically comparable to or lower than the measured  $dB/dt$ , except for slow movement in a strong magnetic field (4–6 s), or when the head turns away from the magnet (> 10 s).

Figure 7 shows the magnitude of the induced electric fields in the CNS and the whole head as a function of time. Three-dimensional visualizations of the induced electric fields in all five anatomical models can be viewed as movie files online (available at [stacks.iop.org/PMB/58/2625/mmedia](http://stacks.iop.org/PMB/58/2625/mmedia)). The spatially maximum peak electric fields in the CNS and in the whole head are on average about  $0.4 \text{ V m}^{-1}$  and  $0.6 \text{ V m}^{-1}$ . The 99th percentile peak electric fields are considerably lower: for the electric field in the CNS, the 99th percentile is on average 60% lower than the maximum value. (The 99 percentile fields are electric



**Figure 8.** The maximum/99th percentile electric field in the CNS (left) and in the whole head (right) divided by the average  $dB/dt$  over the whole head. Horizontal lines show the 95th percentile (solid line) and the median value (dashed line) of the ratio, calculated over all five models and whole time period. Note that for the high peak at 4.8 s, both the electric field and  $dB/dt$  are small.



**Figure 9.** Total induced eddy current (left) and total current divided by the average  $dB/dt$ . In the right figure, horizontal lines show the 95th percentile (solid line) and the median value (dashed line) of the ratio.

field levels which are exceeded only by 1% of computed electric fields.) For the whole head, the 99th percentile is on average 70% lower than the maximum value. In 99 per cent of cases, the maximum electric field is located in cortical bone (in the remaining 1% of cases, the maximum is located in fat). Incidentally, cortical bone is the tissue with the lowest conductivity ( $0.02 \text{ S m}^{-1}$ ). For the CNS tissues, the maximum electric field is located in the grey matter tissue in 96% of cases (remaining 4% in white matter and cerebellum), except for the ELLA model, where the maximum electric field is located in the cerebellum in 75% of cases (remainder in grey matter).

The induced electric field seems to be approximately linearly proportional to the time derivative of the magnetic flux density. This can be seen in figure 8, which shows the ratio between the induced electric field and the average  $dB/dt$  (figure 6) in the head. The figure also shows the median value and 95th percentile of the ratio calculated over all 2000 cases (400 time steps and five models). For a given  $dB/dt$ , a conservative estimate for the induced electric field can be calculated by multiplying the  $dB/dt$  with the 95th percentile of the ratio.

Figure 9 (left) shows the total induced eddy current as a function of time. The highest peak is about  $150 \mu\text{A}$  but usually the current stays below  $100 \mu\text{A}$ . Similarly to the induced electric

field, the total induced eddy current is approximately linearly dependent on the average  $dB/dt$ , which can be seen in figure 9 (right).

## 4. Discussion

### 4.1. Comparison with exposure guidelines

For the comparison of the assessed exposure to limit values in international guidelines we used the recent ICNIRP guidelines for limiting exposure to static (ICNIRP 2009) and time varying (ICNIRP 2010) electric and magnetic fields. Additionally, a draft for electric field induction by a movement in a static magnetic field was available for open consultation (ICNIRP 2012). In normal working environment ICNIRP recommends that the magnetic flux density should not exceed 2 T and the induced electric field should be limited by a threshold below which no stimulation of peripheral nerves and annoying sensations such as vertigo and magnetophosphenes arise (ICNIRP 2009). In specially controlled working conditions 2 T may be exceeded, but annoying sensory effects should be minimized by controlling movements. (From figure 4, it is obvious that 2 T is exceeded by about 50% in this study.) The basic restrictions for the induced electric fields in the ICNIRP (2010) guidelines are given in terms of root-mean-square values; they can be converted into peak values by multiplying them by  $\sqrt{2}$ . For normal occupational exposure, the basic restrictions for CNS tissue of the head are  $0.7/f$  V m<sup>-1</sup> (peak) below 10 Hz and  $0.07$  V m<sup>-1</sup> from 10 to 25 Hz ( $f$  is the frequency in Hertz). Below the frequency of 1 Hz, it is assumed that the basic restriction for the CNS increases as  $0.7/f$  V m<sup>-1</sup>, until it reaches the limit of  $1.1$  V m<sup>-1</sup> (the basic restriction for all tissues). For controlled exposure, the basic restriction for all tissues of the head and body is  $1.1$  V m<sup>-1</sup> (peak) independent of frequency, which is based on preventing stimulation of peripheral nervous system (PNS).

According to ICNIRP (2010), the 99th percentile electric field for each specific tissue is the relevant value to be compared with the basic restrictions. The rationale for employing the 99th percentile electric field for the basic restrictions has been to reduce the numerical stair-casing error. In this work, the stair-casing error has been reduced by other means: by removing sharp conductivity contrasts as described in Laakso and Hirata (2012c), and spatially averaging the electric field over  $2\text{ mm} \times 2\text{ mm} \times 2\text{ mm}$  volumes (64 voxels). This technique has been shown to provide numerically reliable values for the spatial maximum electric field (Laakso and Hirata 2012a). Additionally, there are difficulties in calculating the 99th percentile separately for each tissue (section 2.6), and, as the distribution of  $dB/dt$  is nonuniform, the 99th percentile electric field might considerably underestimate the exposure compared to the spatial maximum electric field (Laakso and Hirata 2012a, 2012c). Therefore, in the following both the spatial maximum and 99th percentile electric fields are compared with the basic restrictions.

As seen in figure 7 (right), the PNS limit of  $1.1$  V m<sup>-1</sup> for the induced electric field is not exceeded in any of the five models for the head trajectory considered herein. As shown in figure 8, a conservative estimate that holds in 95% of cases for the 99th percentile electric field is  $0.11$  V m<sup>-1</sup> for an average  $dB/dt$  of  $1$  T s<sup>-1</sup>. Thus, the 99th percentile electric fields are unlikely to violate the basic restriction until the average  $dB/dt$  in the head exceeds  $10$  T s<sup>-1</sup>. From figure 8, a conservative estimate for the spatial maximum electric field is  $0.40$  V m<sup>-1</sup> for an average  $dB/dt$  of  $1$  T s<sup>-1</sup>. If the spatial maximum value is compared with the basic restriction instead of the 99th percentile value, the basic restriction is unlikely to be exceeded for an average  $dB/dt$  lower than about  $3$  T s<sup>-1</sup>. It should be noted that the induced electric fields elsewhere in the body may be higher than those in the head.

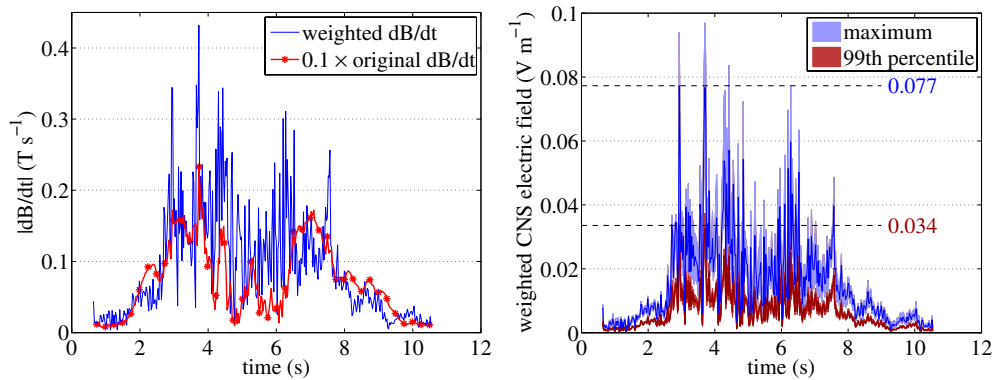


**Figure 10.** Weighted average  $dB/dt$  compared to the unweighted average  $dB/dt$  (left). The maximum and 99th percentile weighted electric fields in the CNS (right). The reference frequency for weighting is 10–25 Hz. In the right figure, solid lines show the average values and the shaded areas depict the ranges of variation over the five anatomical models.

However,  $dB/dt$  is likely to be higher in the head than in the trunk (Fuentes *et al* 2008, de Vocht *et al* 2009).

As the basic restriction for the electric field in the CNS depends on the frequency, the electric field induced in the CNS shown in figure 7 (left) cannot be directly compared with it. Instead, the induced electric field needs to be converted into a weighted field that depends on the ‘waveform’ of the field (ICNIRP 2010). The weighted field is determined by first calculating the spectrum of the induced electric field by the discrete Fourier transform, then filtering the spectrum with a piecewise linear weighting function described in ICNIRP (2010), and finally applying the inverse Fourier transform to the filtered spectrum. The weighting function that is used for filtering the spectrum depends on an arbitrarily chosen reference frequency (in this work: 10–25 Hz). The weighted field should be compared with the basic restriction at this frequency. For realistic movements in a nonuniform static magnetic field, the time dependency of the electric field is different in each point of the head. Consequently, the weighted electric field would need to be calculated separately for each point, which would not be practical. Therefore, for the purpose of comparison with the basic restriction, we have assumed that the electric field everywhere in the head has the same time-dependency as the average  $dB/dt$  in the head. Then, the weighted electric field can be calculated by first calculating the weighted  $dB/dt$ , shown in figure 10 (left), and then scaling the unweighted electric field in figure 7 (left) by the ratio between the weighted  $dB/dt$  and the original  $dB/dt$ . The weighted electric field calculated in this way for a reference frequency of 10–25 Hz is shown in figure 10 (right). The highest weighted 99th percentile and spatial maximum electric fields are on average 0.034 and 0.077  $V m^{-1}$ . The former is about one half of the basic restriction of 0.07  $V m^{-1}$ , and the latter slightly exceeds the basic restriction. When compared with the basic restriction for the PNS that was discussed in the previous paragraph, the basic restriction for the CNS seems to be more restrictive. Figure 8 shows that conservative estimates for the 99th percentile and spatial maximum electric fields in the CNS are 0.09 and 0.23  $V m^{-1}$  for a  $dB/dt$  of 1  $T s^{-1}$ . Thus, when the weighted peak  $dB/dt$  is less than 0.8  $T s^{-1}$  or 0.3  $T s^{-1}$  (reference frequency of 10–25 Hz), the 99th percentile and spatial maximum electric fields, respectively, are unlikely to exceed the basic restrictions. As discussed above, the weighted peak  $dB/dt$  should be determined from the time course of  $dB/dt$  using frequency-dependent filtering.

#### 4.2. Implications on occupational exposure assessment

The magnitude of the induced electric field and current were approximately linearly related to the average value of  $dB/dt$  in the head, independent of the position of the head with respect to the magnet. This suggests that the average  $dB/dt$  is a good metric for the exposure to movement induced electric fields. Additionally, it was observed that  $dB/dt$  measured using a probe attached to the forehead gives conservative estimates for the average  $dB/dt$  inside the head, provided that the head of the subject is pointing towards higher magnetic field. These observations support the use of a  $dB/dt$  probe for occupational exposure measurements.

Personal portable dosimeters have been utilized for measuring the exposure of workers to static magnetic field and  $dB/dt$  in several studies (de Vocht *et al* 2009, Fuentes *et al* 2008, Bradley *et al* 2007). Each of these studies considered multiple MRI systems with magnet strengths ranging from 1 T to 4 T. The subjects included workers at an MRI manufacturing plant (de Vocht *et al* 2009), and workers operating an MRI system in a clinical or research setting (Fuentes *et al* 2008, Bradley *et al* 2007). During normal work tasks, the highest measured static magnetic flux densities were 1.4 T (Fuentes *et al* 2008), 1.1 T (de Vocht *et al* 2009), and 0.8 T (Bradley *et al* 2007), which are lower than those reported in this study and do not exceed 2 T, which is the ICNIRP recommendation for normal working conditions (ICNIRP 2009). However, the maximum measured  $dB/dts$  were in the range of 4–5  $T s^{-1}$  (Fuentes *et al* 2008, de Vocht *et al* 2009), which are higher than the maximum average  $dB/dt$  of 2.5  $T s^{-1}$  considered in this study. It should be noted that in the above studies, the dosimeter was worn at waist; both the static magnetic flux density and  $dB/dt$  are likely to be even higher in the head (de Vocht *et al* 2009). For instance, Fuentes *et al* (2008) measured  $dB/dt$  near the head during a bending motion at the edge of the magnet bore for 1.5, 2, and 4 T magnets. The highest  $dB/dt$  were 7.3  $T s^{-1}$ , 4.4  $T s^{-1}$ , and 6.2  $T s^{-1}$ , respectively, which are considerably higher compared to this study. In summary, it seems that for certain tasks routinely performed by MRI workers,  $dB/dt$  may be more than a factor of two higher than the  $dB/dt$  considered in this study. As discussed in the previous section, the basic restrictions for the induced electric field are close to being or are exceeded for the path of movement of this study. It is therefore clear that the movement-induced electric field may well exceed the basic restriction during some usual work tasks.

#### 4.3. Magnetic field induced vertigo

The magnitude of the eddy current that was induced in the head was in the range of 50  $\mu A$  for a  $dB/dt$  of 1  $T s^{-1}$ . For the path of movement considered in this study, the highest induced current was about 150  $\mu A$ . It is reasonable to assume that for quicker movements (the volunteer tried to avoid sudden movements) or stronger magnets, the induced current reaches magnitudes ( $\gtrsim 500 \mu A$ ) that have been used for GVS (Fitzpatrick and Day 2004). For instance, fast head rotations just inside the magnet bore can generate a  $dB/dt$  between 10 and 20  $T s^{-1}$  (Glover *et al* 2007). Therefore, the role of induced currents in the generation of magnetic-field induced vertigo cannot be ruled out. In GVS, direct currents applied to electrodes attached to the skin behind the outer ears are used for disturbing the function of the vestibular system. As no study has accurately modelled the path of the current through the head and inner ears, it is unclear how strong electric field/current density at the vestibular system is needed for producing observable effects on balance. Perilymphic and endolymphic fluids, which fill the bony and membranous labyrinths of the inner ear, have a relatively high conductivity that may be comparable to that of the CSF (Parazzini *et al* 2007). Consequently, the path of the induced/applied current might be 'attracted' towards the inner ears, which would result in

a local maximum of the current density. However, none of the anatomical models used in this study featured models for the inner ears; thus, for testing this hypothesis, more studies that properly model the inner ears are needed. Note that in the study of Roberts *et al* (2011), who observed effects of the static magnetic field on eye movements but no effects of  $dB/dt$ ,  $dB/dt$  was at most  $3.5 \text{ T s}^{-1}$ . In the study of Glover *et al* (2007), no vertigo was observed for stationary subjects who were exposed to a  $dB/dt$  of  $2.0 \text{ T s}^{-1}$  for a duration of 200 ms or a  $dB/dt$  of  $5.0 \text{ T s}^{-1}$  for 40 ms.

#### 4.4. Sources of uncertainty

This study employed the exact same computational method as Laakso and Hirata (2012a), where some of the sources of uncertainty that affect the computed results were investigated. For example, it was shown that the numerical error due to the resolution of the computation grid only has minor effect in the range of  $\pm 10\%$ . As discussed in Laakso and Hirata (2012a), several investigators have employed widely varying values for the tissue conductivities, especially for brain tissues. In this work, the conductivities of the grey and white matters and cerebellum were assumed to be 0.10, 0.06, and  $0.10 \text{ S m}^{-1}$ , respectively. According to Laakso and Hirata (2012a), if the conductivities of brain tissues are increased by  $+100\%$ , the 99th percentile and maximum electric fields in the brain may decrease by up to  $-30\%$  or  $-40\%$ , respectively. Likewise, if the conductivity of the brain is reduced to one half, the electric fields may increase by up to  $+30\%$  or  $+50\%$ . Similar variations are expected for other tissues, too. For example, the maximum electric field was almost always located in the skull ( $0.02 \text{ S m}^{-1}$ ), so altering the conductivity of the skull would naturally have a great impact on the maximum electric field values. It is therefore essential to carefully consider the choice of conductivity values when comparing results of different computational studies. Note that the error due to neglecting the displacement current is likely to be much smaller than the uncertainties in conductivity values (Barchanski *et al* 2005).

Only one trajectory of the head was investigated in this study. It should be noted that both the speed and direction of translational and rotational motions and also the distribution of the static magnetic field varied along the trajectory. Nevertheless, the ratio between the induced electric field/current and  $dB/dt$  was relatively constant (figures 8 and 9). Therefore, even for different trajectories, it is reasonable to assume that the ratio between the induced electric field/current and  $dB/dt$  would fall within the range predicted in this study. This study considered five different anatomical models, which were originally developed by three different research groups. The number of models is too small for statistical analysis, but the results still provide some insight into variations between different anatomical models. In figure 7, average variation ranges (over 400 time steps) as the percentage difference from the mean value (over five models) are  $-10\% \dots +10\%$  for the 99th percentile electric field, and  $-20\% \dots +20\%$  for the maximum electric field. It is unclear how much of this variation is attributable to real anatomical differences and how much to potential numerical artefacts, such as errors in tissue segmentation. Also, it should be noted that the variation ranges might expand if more anatomical models were taken into consideration.

One of the approximations that requires further discussion is excluding the body from the neck down from consideration. For investigating the impact of this approximation, the induced electric field was computed for the exposure to a uniform slowly-varying lateral magnetic field for all five models. Excluding the body underestimated the maximum and 99th percentile induced electric fields in the CNS tissue of the head by at most 2%. For the 99th percentile and maximum electric fields calculated over the whole head and neck, the underestimation was, at most, 4%. The total induced current in the head was underestimated by, at most, 6%.

These underestimations are smaller than, for instance, variations between different anatomical models.

## 5. Conclusions

Movement induced fields were investigated in five anatomically realistic models of the human head. The workflow for determining the induced electric field consisted of magnetic field measurements, modelling the magnetic field of the MRI scanner, modelling the trajectory of movement based on the measured and modelled magnetic fields, and finally numerically calculating the induced electric field using the finite-element method. The maximum and 99th percentile induced electric fields in the head were approximately linearly dependent on the average time derivative of the magnetic flux density ( $dB/dt$ ) in the head. This supports the use of  $dB/dt$  measurements for assessing the exposure to movement induced fields. Conservative estimates for the spatial maximum and 99th percentile electric fields in the whole head were 0.40 and 0.11 V m<sup>-1</sup> for a  $dB/dt$  of 1 T s<sup>-1</sup>. For the CNS tissues, the corresponding estimates were 0.23 and 0.09 V m<sup>-1</sup>. It should be noted that when comparing the electric field calculated from these estimates with the basic restriction for the CNS, the field should be spectrally weighted as described in ICNIRP (2010). For the path of movement of this study, the spatial maximum electric fields in the whole head and in the CNS were close to or slightly exceeded the respective basic restrictions. The 99th percentile electric field, which was less restrictive than the spatial maximum by a factor of approximately three, did not exceed the basic restrictions. However, significantly higher values of  $dB/dt$  than those considered in this study have been reported in previous literature. Therefore, it seems that not only the spatial maximum but also the 99th percentile electric field might exceed the basic restrictions during some usual tasks performed by MRI workers. It was also found that the induced eddy currents are within the same order of magnitude as currents that have been used for electrical stimulation of the vestibular function. This supports the assumption that the movement induced electric fields have a significant role in the generation of magnetic field induced vertigo.

## Acknowledgments

IL wishes to thank the Finnish Cultural Foundation and the Academy of Finland for financial support.

## References

- Bakker J F, Paulides M M, Neufeld E, Christ A, Chen X L, Kuster N and van Rhoon G C 2012 Children and adults exposed to low-frequency magnetic fields at the ICNIRP reference levels: theoretical assessment of the induced electric fields *Phys. Med. Biol.* **57** 1815–29
- Barchanski A, Gersem H D, Gjonaj E and Weiland T 2005 Impact of the displacement current on low-frequency electromagnetic fields computed using high-resolution anatomy models *Phys. Med. Biol.* **50** N243–9
- Baumann S, Wozny D, Kelly S and Meno F 1997 The electrical conductivity of human cerebrospinal fluid at body temperature *IEEE Trans. Biomed. Eng.* **44** 220–3
- Bradley J K, Nyekiova M, Price D L, Lopez L D and Crawley T 2007 Occupational exposure to static and time-varying gradient magnetic fields in MR units *J. Magn. Reson. Imaging* **26** 1204–9
- Bringuiet E 2003 Electrostatic charges in  $v \times B$  fields and the phenomenon of induction *Eur. J. Phys.* **24** 21–29
- Chiampì M and Zilberti L 2011 Induction of electric field in human bodies moving near MRI: an efficient BEM computational procedure *IEEE Trans. Biomed. Eng.* **58** 2787–93
- Christ A *et al* 2010 The virtual family—development of surface-based anatomical models of two adults and two children for dosimetric simulations *Phys. Med. Biol.* **55** N23–38

- Cobos Sánchez C, Bowtell R W, Power H, Glover P, Marin L, Becker A A and Jones A 2009 Forward electric field calculation using BEM for time-varying magnetic field gradients and motion in strong static fields *Eng. Anal. Bound. Elem.* **33** 1074–88
- Cobos Sánchez C, Glover P, Power H and Bowtell R 2012 Calculation of the electric field resulting from human body rotation in a magnetic field *Phys. Med. Biol.* **57** 4739–53
- Crozier S and Liu F 2005 Numerical evaluation of the fields induced by body motion in or near high-field MRI scanners *Prog. Biophys. Mol. Biol.* **87** 267–78
- de Vocht F, Muller F, Engels H and Kromhout H 2009 Personal exposure to static and time-varying magnetic fields during MRI system test procedures *J. Magn. Reson. Imaging* **30** 1223–8
- de Vocht F, van Drooge H, Engels H and Kromhout H 2006 Exposure, health complaints and cognitive performance among employees of an MRI scanners manufacturing department *J. Magn. Reson. Imaging* **23** 197–204
- Dimbylow P J 1998 Induced current densities from low-frequency magnetic fields in a 2 mm resolution, anatomically realistic model of the body *Phys. Med. Biol.* **43** 221–30
- Fitzpatrick R C and Day B L 2004 Probing the human vestibular system with galvanic stimulation *J. Appl. Physiol.* **96** 2301–16
- Fuentes M, Trakic A, Wilson S and Crozier S 2008 Analysis and measurements of magnetic field exposures for healthcare workers in selected MR environments *IEEE Trans. Biomed. Eng.* **55** 1355–64
- Gabriel C 1996 Compilation of the dielectric properties of body tissues at RF and microwave frequencies *Technical Report AL/OE-TR-1996-0037* Armstrong Laboratory (AFMC), Occupational and Environmental Health Directorate, Radiofrequency Radiation Division, Brooks Air Force Base, TX, USA (<http://niremf.ifac.cnr.it/docs/DIELECTRIC/home.html>)
- Glover P M and Bowtell R 2008 Measurement of electric fields induced in a human subject due to natural movements in static magnetic fields or exposure to alternating magnetic field gradients *Phys. Med. Biol.* **53** 361–73
- Glover P M, Cavin I, Qian W, Bowtell R and Gowland P 2007 Magnetic-field-induced vertigo: a theoretical and experimental investigation *Bioelectromagnetics* **28** 349–61
- Heilmaier C, Theysohn J M, Maderwald S, Kraff O, Ladd M E and Ladd S C 2011 A large-scale study on subjective perception of discomfort during 7 and 1.5 T MRI examinations *Bioelectromagnetics* **32** 610–9
- ICNIRP 2009 Guidelines on limits of exposure to static magnetic fields *Health Phys.* **96** 504–14
- ICNIRP 2010 Guidelines for limiting exposure to time-varying electric and magnetic fields (1 Hz to 100 kHz) *Health Phys.* **99** 818–36
- ICNIRP 2012 Draft guidelines for limiting exposure to electric fields induced by movement of the human body in a static magnetic field and by time-varying magnetic fields below 1 Hz (<http://www.icnirp.org/OpenMovement/ICNIRPMovementConsultationDraft2012.pdf>)
- IEEE 2002 IEEE standard for safety levels with respect to human exposure to electromagnetic fields, 0–3 kHz, C95.6-2002
- Iivonen S and Laakso I 2009 Computational estimation of magnetically induced electric fields in a rotating head *Phys. Med. Biol.* **54** 341–51
- Jokela K and Saunders R D 2011 Physiologic and dosimetric considerations for limiting electric fields induced in the body by movement in a static magnetic field *Health Phys.* **100** 641–53
- Kännälä S, Toivo T, Alanko T and Jokela K 2009 Occupational exposure measurements of static and pulsed gradient magnetic fields in the vicinity of MRI scanners *Phys. Med. Biol.* **54** 2243–57
- Laakso I and Hirata A 2012a Computational analysis of thresholds for magnetophosphenes *Phys. Med. Biol.* **57** 6147–65
- Laakso I and Hirata A 2012b Fast multigrid-based computation of the induced electric field for transcranial magnetic stimulation *Phys. Med. Biol.* **57** 7753–65
- Laakso I and Hirata A 2012c Reducing the staircasing error in computational dosimetry of low-frequency electromagnetic fields *Phys. Med. Biol.* **57** N25–34
- Lindenblatt G and Silny J 2001 A model of the electrical volume conductor in the region of the eye in the ELF range *Phys. Med. Biol.* **46** 3051–59
- Liu F, Zhao H and Crozier S 2003 Calculation of electric fields induced by body and head motion in high-field MRI *J. Magn. Reson.* **161** 99–107
- Nagaoka T, Watanabe S, Sakurai K, Kunieda E, Watanabe S, Taki M and Yamanaka Y 2004 Development of realistic high-resolution whole-body voxel models of Japanese adult males and females of average height and weight, and application of models to radio-frequency electromagnetic-field dosimetry *Phys. Med. Biol.* **49** 1–15
- Parazzini M, Tognola G, Franzoni C, Grandori F and Ravazzani P 2007 Modeling of the internal fields distribution in human inner hearing system exposed to 900 and 1800 MHz *IEEE Trans. Biomed. Eng.* **54** 39–48
- Roberts D, Marcelli V, Gillen J, Carey J, Della Santina C and Zee D 2011 MRI magnetic field stimulates rotational sensors of the brain *Curr. Biol.* **21** 1635–40

- Schenck J F 2000 Safety of strong, static magnetic fields *J. Magn. Reson. Imaging* **12** 2–19
- Shellock F G and Crues J V 2004 MR procedures: biologic effects, safety, and patient care *Radiology* **232** 635–52
- van Nierop L E, Slottje P, van Zandvoort M J E, de Vocht F and Kromhout H 2012 Effects of magnetic stray fields from a 7 Tesla MRI scanner on neurocognition: a double-blind randomised crossover study *Occup. Environ. Med.* **69** 759–66
- Weintraub M I, Khoury A and Cole S P 2007 Biologic effects of 3 tesla (T) MR imaging comparing traditional 1.5 T and 0.6 T in 1023 consecutive outpatients *J. Neuroimaging* **17** 241–5